Applied Catalysis B: Environmental 129 (2013) 48–55

Contents lists available at SciVerse ScienceDirect

Applied Catalysis B: Environmental

journal homepage: www.elsevier.com/locate/apcatb

Enhanced photoactivity of Cu-deposited titanate nanotubes for removal of bisphenol A

Ruey-an Doong [a,*], Sue-min Chang [b,**], Chia-wei Tsai [a]

[a] Department of Biomedical Engineering and Environmental Sciences, National Tsing Hua University, 101, Sec. 2, Kuang Fu Road, Hsinchu 30013, Taiwan
[b] Institute of Environmental Engineering, National Chiao Tung University, 1001, University Road, Hsinchu 30010, Taiwan

ARTICLE INFO

Article history:
Received 3 May 2012
Received in revised form 4 September 2012
Accepted 9 September 2012
Available online 16 September 2012

Keywords:
Copper ions
Titanate nanotubes (TNTs)
Bisphenol A
Photodeposition
Photocatalytic activity

ABSTRACT

One-dimensional nanotubes are promising nanostructured materials for a wide variety of environmental applications. In this study, the Cu-deposited titanate nanotubes (TNTs) were fabricated using an alkaline hydrothermal method at 150 °C and then 0.5–2 wt% Cu(II) ions were photodeposited onto the calcined TNTs at 500 °C for enhanced photodegradation of bisphenol A (BPA) under illumination of 365 nm UV light. The as-synthesized TNTs showed tubular structures with the outer diameter and inter-layer spacing of 7–10 and 0.8 nm, respectively. The X-ray absorption near-edge spectral results provided a strong support on the partially structural change from layered trititanate to anatase TiO_2 through the distortion of octahedral TiO_6 unit at 500 °C and the production of mixture of CuO and Cu_2O after photodeposition of Cu ions, resulting in the formation of Cu-deposited TiO_2/TNT nanocomposites to enhance the photocatalytic activity. A nearly complete removal of BPA by the Cu-deposited TiO_2/TNTs was observed, and the pseudo-first-order rate constants (k_{obs}) for BPA photodegradation by Cu-deposited TiO_2/TNTs at pH 7.0 were 1.8–5.2 and 4.3–12.7 times higher than those of pure Degussa P25 and ST01 TiO_2, respectively. In addition, the k_{obs} for BPA photodegradation reached the maximum value of $0.253 \pm 0.032\ min^{-1}$ at 1 wt% Cu(II). The X-ray photoelectron spectra showed that the ratio of Cu_2O to total Cu increased from 3.2% in the dark to 35.2% after illumination of 365 nm UV light for 5 min. In addition, electron paramagnetic resonance results indicated that the copper ions could serve as the electron mediators to prolong the retention time of photo-generated radicals, resulting in the enhancement of photodegradation efficiency and rate of BPA by Cu-deposited TiO_2/TNTs.

1. Introduction

The development of efficient photocatalysts for removal of emerging pollutants has received considerable attention for treatment of recalcitrant compounds in water and wastewater. Nanostructured TiO_2 is one of the most promising materials widely used in photocatalytic and photovoltaic technologies [1]. In addition to TiO_2 nanoparticles, the one-dimensional (1D) titanate nanotubes (TNTs) are promising nanostructured materials for energy and environmental applications [2,3]. The fabrication of TNTs has been extensively studied and alkaline hydrothermal treatment is one of the most often used methods for preparation of TNTs due to the low cost and simplicity [3–5]. However, the TNTs prepared by the alkaline hydrothermal treatment are H-titanate forms and show inferior performance on photodegradation of pollutants when compared with that of Degussa P25 TiO_2 [1,6].

Several strategies have been developed for enhancement of photocatalytic ability of TNTs. A suitable and feasible strategy to retain the photocatalytic activity of TNTs is the post-thermal treatment to form well-crystallized TiO_2 while still retaining the tubular structures [7]. Several studies have demonstrated the enhanced photocatalytic activity of calcined TNT towards organic dye photodegradation [8–10]. Addition of transition metal ions as dopants to decrease the recombination rate or to shift the adsorption wavelength is another promising method to improve the degradation efficiency and rate of organic pollutants in aqueous solutions. Several studies have depicted that addition of metal ions such as V, Zr, Fe, Ag, Co, and Cu could enhance the photodegradation efficiency of titanium-based materials [11–14]. The Cu(II) ion is one of the effective catalytic species for the enhancement of photocatalytic activity of TiO_2 [15,16]. Doong et al. [16] depicted that Cu(II) can be reduced to the low-valent species in the presence of formate and then deposited on the surface of TiO_2, resulting in the decrease in electron-hole recombination rate and the acceleration of electron transfer rate to enhance the photodegradation efficiency and rate of methylene blue. Several metal ions including Ag, Pt, and Fe have also been

* Corresponding author. Tel.: +886 35726785; fax: +886 35718649.
** Corresponding author.
E-mail address: radoong@mx.nthu.edu.tw (R.-a. Doong).

0926-3373/$ – see front matter © 2012 Elsevier B.V. All rights reserved.
http://dx.doi.org/10.1016/j.apcatb.2012.09.011

employed to enhance the photodegradation efficiency and rate of CO, methylene orange, and acetone by 1D nanostructured titanates [17–19]. However, the effect of Cu ions on the enhanced photoactivity of TNTs towards emerging pollutant degradation remains unclear.

Endocrine disrupting chemicals such as bisphenol A (BPA), estradiol, and estrone are typical emerging pollutants commonly found in the aquatic environments [20,21]. BPA is a known chemical used for manufacturing polycarbonate resins and stabilizing plastics. This compound can be easily released into the environment through the domestic sewages and industrial wastewaters, which may cause endocrine-disruptive effects on human beings and aquatic biota [22]. Various technologies including adsorption [23], chemical oxidation [24], advanced oxidation processes [25,26], and photocatalysis [27–29] have been developed to remove BPA from water and wastewater. Among the technologies developed, photocatalytic oxidation is one of the most effective methods for elimination of BPA in aqueous solutions [28]. Guo et al. [29] used three-dimensional mesoporous TiO_2 nanocatalysts to photodegrade BPA and found that the degradation rate of BPA by mesoporous TiO_2 was 4 times higher than that by Degussa P25 TiO_2. However, the photocatalytic degradation of BPA by 1D Cu-deposited nanomaterials has rarely reported.

In this study, the Cu-deposited TNTs were fabricated using an alkaline hydrothermal method and calcined at 500 °C for 4 h to form TiO_2/TNT nanocomposites. The 0.5–2 wt% Cu ions were then photo-deposited onto the TiO_2/TNT surfaces for enhanced photodegradation of BPA. The morphology as well as microstructures of as-synthesized and Cu-deposited TiO_2/TNTs including surface area, pore texture, and crystallinity were characterized by scanning/transmission electron microscopy (SEM/TEM), surface area analysis, X-ray diffractometry (XRD), and X-ray absorption near-edge spectroscopy (XANES). The photocatalytic activity of Cu-deposited TiO_2/TNTs towards BPA degradation was further evaluated. In addition, the change in photo-generated radicals were also measured to elucidate the possible role of Cu(II) ions in photodegradation of BPA by Cu-deposited TiO_2/TNTs.

2. Materials and methods

2.1. Chemicals

All chemicals were used as received without further treatment. ST01 TiO_2 powder was obtained from Ishihara Sangyo Ltd. (Tokyo, Japan). Sodium hydroxide pellets (NaOH) and copper(II) nitrate pentahemihydrate ($Cu(NO_3)_2{\cdot}2.5H_2O$, 98%) were purchased from Riedel-de Haën (Seelze, Germany). Hydrochloric acid (36.5–38.0%) was purchased from J.T. Baker (Phillipsburg, NJ). Bisphenol A (99+% purity) was purchased from Aldrich. All solutions were prepared with high-purity bidistilled deionized water (Millipore Co., 18.3 MΩ cm) unless otherwise mentioned.

2.2. Fabrication of Cu-deposited TNTs

The 1D nanostructured TNTs were synthesized by a hydrothermal method using ST-01 TiO_2 as the starting material. In general, 1.6 g of ST01 TiO_2 powders were dispersed into 20 mL of 10 M NaOH in a 30 mL-Teflon-lined vessel. The suspension was ultrasonicated for 1 h at room temperature and then the hydrothermal reaction were carried out at 150 °C for 24 h. After cooling down to room temperature, the hydrothermal products were washed with 0.1 N HCl and bidistilled water repeatedly until the pH of solution was around 7.0. Ethanol was then used to replace water, and the hydrothermal products were separated from the washing solution by filtration, dried at 60 °C for 10 h in oven. The as-synthesized TNTs were then calcined at 500 °C in air for 4 h to form TiO_2/TNT nanocomposites.

The Cu-deposited TiO_2/TNTs were prepared by the photodeposition method. Typically, 1 g/L of calcined TiO_2/TNT composites were dispersed in distilled water under vigorous stirring, and various amounts of $Cu(NO_3)_2$ solution were added into the solution to get the final concentrations of 5–40 mg/L Cu(II). The suspension was irradiated by 365 nm UV light for 4 h at 25 °C, and the obtained Cu-deposited TiO_2/TNTs were harvested by filtration, dried at 60 °C for 10 h in oven. The Cu(II) concentrations in filtrates were then determined by inductively coupled plasma optical emission spectroscopy, and the aqueous Cu(II) concentration was 0.25, 9.6 and 18.4 mg/L when the added Cu(II) concentrations were 5, 20 and 40 mg/L, respectively, which indicates that the deposited amounts of Cu(II) onto the TiO_2/TNT nanocomposites were *ca.* 0.5, 1 and 2 wt%. In addition, the obtained Cu-deposited TiO_2/TNTs were stored in the glove box under N_2 atmosphere until analysis to minimize the oxidation of copper species.

2.3. Photocatalytic activity of BPA by Cu-deposited TiO_2/TNTs

The photocatalytic degradation reaction was carried out in a hollow cylindrical photoreactor equipped with a water jacket. The inner wall of the water jacket is made of fused silica and the outer wall is made of Pyrex. Four 8 W black light blue lamps (BLB lamp, -8T5, Winstar Lighting Co., Taipei, Taiwan) with 365 nm as the major peak wavelength were used as the light source and positioned within an inner part of the photoreactor encompassing 4 quartz tubes. The reactor was cooled by circulating water through a Pyrex jacket and maintained the temperature at 25 °C. The 1 g/L titanium-based nanomaterials including Cu-deposited TiO_2/TNTs and commercial TiO_2 nanoparticles were added in a 15 mL of BPA solution. Prior to the illumination, the suspension was magnetically stirred in the dark for 30 min to ensure the adsorption equilibrium of BPA onto the catalysts. After the equilibrium, the UV light was turned on and aliquots (1 mL) were withdrawn from the solution at various time intervals for analysis after removal of catalysts by centrifugation at 14,000 rpm for 5 min. After centrifugation, 0.5 mL of supernatant of each sample was transferred to a 2 mL HPLC vial and the aqueous concentration of BPA was determined by a high-performance liquid chromatograph (HPLC) equipped with C-18 column (LUNA 5u 100A, 4.6 mm × 250 mm, Phenomenex) and a diode array detector (HPLC-DAD, Agilent Technologies, series 1200). The isocratic methanol/acetonitrile/water mixture (50:30:20, v/v) at a flow rate of 0.5 mL/min was used as the elute. In addition, absorbance at 225 nm was used to determine the BPA concentration.

2.4. Reaction kinetics

It is known that the rate of photocatalytic degradation of organic pollutants at liquid-solid interface can be described by the Langmuir-Hinshelwood kinetic model [13,30]:

$$r_o = \frac{dC}{dt} = k_{\text{app}} \frac{K_F S_t C}{1 + K_F C} \quad (1)$$

where r_o is the reaction rate of BPA photodegradation, C is the aqueous concentration of BPA, k_{app} is the limiting-step rate constant of reaction at maximum coverage under the given conditions, S_t is the total reaction sites of Ti-based nanomaterials, and K_F is the

adsorption coefficient of BPA. When the BPA concentration (C) is low, Eq. (1) can be simplified to the pseudo-first-order kinetics:

$$\ln\left(\frac{C}{C_o}\right) = -k_{obs}t \quad (2)$$

where k_{obs} is the pseudo-first-order rate constant for BPA photodegradation (min^{-1}).

2.5. Characterization

The surface morphology of as-synthesized and Cu-deposited TiO_2/TNTs was characterized by SEM (JEOL JSM-6700F OXFORD INCA ENERGY 400). All the samples were Pt-coated using Ion Sputter ε-1030 (Hitachi, Tokyo) to increase the conductivity of the sample surface. After coating with Pt, samples were placed under high vacuum (10^{-3}–10^{-7} mbar) conditions. An acceleration electron voltage of 5 kV was applied to obtain the SEM images. In addition, the dimension and morphology of nanostructured titanate materials were examined by TEM (JEOL, JEM-2010) and high resolution transmission electron microscopy (HRTEM, JEOL, JEM-3000F) at accelerating voltages of 200 and 300 kV, respectively.

The Brunauer–Emmett–Teller (BET) specific surface area and pore size distribution were carried out by nitrogen adsorption and desorption at 77 K using a surface area and porosimetry system (ASAP 2020, Micromeritics). In addition, pore, radii and volumes of the nanostructured materials can be determined using Barrett, Joyner and Halenda's (BJH) mathematical models. The BJH method for calculating pore size distributions is based on a model of the adsorbent as a collection of cylindrical pores.

The crystalline structures were identified by XRD using X-ray diffractometer (Bruker NEW D8 ADVANCE, Germany) with a Lynx eye high-speed strip detector and Ni-filtered Cu Kα radiation (λ = 1.5406 Å) operating at a generator voltage and an emission current of 40 kV and 40 mA, respectively. The X-ray diffraction patterns were acquired over the 2θ ranging from 20° to 90° with sampling step width of 0.05° (step time = 0.5 s).

The X-ray adsorption near-edge structure (XANES) spectra of Ti K-edge and Cu $L_{2,3}$-edge were measured using BL-16A and BL-20A, respectively, at National Synchrotron Radiation Research Center (NSRRC, Hsinchu, Taiwan) in which the electron storage ring was operated at 1.5 GeV with a beam current of 300 mA. The Ti K-edge absorption spectra were measured in a total X-ray fluorescence yield mode at room temperature using a Lytle detector with powder sample dispersed onto Kapton tape. X-rays were monochromated by using a Si(1 1 1) double monochromator before reflecting off a higher-order harmonic light rejection mirror. The photon energies were calibrated using the L_3-edge of a Mo foil at 2520 eV. Energy steps as small as 0.2 eV were employed near the absorption edges with an accounting time of 2 s per step. In addition, the Cu $L_{2,3}$-edge absorption spectra were detected using high-energy spherical grating monochromator beam-line with a micro-channel-plate detector system. The photon energy was calibrated with 0.1 eV using the Cu L_3 white line at 931.2 eV of a CuO reference.

The photo-generated free radicals from the photodegradation of BPA by Cu-deposited TiO_2/TNTs in the presence of 4.4 mM 5,5-dimethyl-1-pyrroline N-oxide (DMPO) was examined using an electron paramagnetic resonance (EPR) spectrometer (Bruker, EMX-10, Germany) working at X-band frequency of 9.49–9.88 GHz with power of 8.02 mW. A 250 W Xe lamp (Ushio Inc.) at major output wavelength of 365 nm was equipped to the sample cavity by lined optical fiber. Oxygen-saturated Cu-deposited TiO_2/TNT suspensions containing DMPO and BPA were irradiated with UV light at room temperature. After irradiated for 5–30 min, the spectra of trapped charges in solutions were recorded at room temperature. The instrumental conditions were set at a center field of 3400–3510 G and a sweep width of 200 G.

3. Results and discussion

3.1. Characterization of as-synthesized and calcined TNTs

Fig. 1 and Fig. S1 show the SEM and TEM images of as-synthesized TNTs and Cu-deposited TiO_2/TNTs. The as-synthesized TNTs showed tubular structures with lengths of few μm (Fig. 1a and Fig S1a). In addition, the TEM and HRTEM images of the as-synthesized TNTs exhibited uniform diameters along with the length (Fig. 1b). The open-ended and multi-layered tubular structures of as-synthesized TNTs shown in TEM images indicated that the inner and outer diameters were 4–6 and 7–10 nm, respectively, with interlayer spacing was about 0.8 nm, which are in good agreement with the previous report [4]. After post-thermal treatment at 500 °C for 4 h and deposition of Cu ions, an obvious change in surface morphology was observed in which the tubular structures and nanoparticles coexisted (Fig. S1b). The TEM images of Cu-deposited TiO_2/TNTs showed the production of well-crystallized nanoparticles on the tube walls (Fig. 1c). In addition, the EDS analysis indicated that the nanocomposites contained Ti, O and Cu (Fig. 1d), which means that the Cu species has deposited onto the surface of TNTs.

The microstructures of as-synthesized TNTs and Cu-deposited TiO_2/TNTs including crystallinity, surface area, and pore structure were further examined. The XRD patterns of the as-synthesized TNTs showed peaks centered at 9.5°, 24.1°, 28.3°, and 48.2° 2θ (Fig. 2). No anatase peak appeared, which indicates the complete conversion of ST01 TiO_2 to 1D layered trititanate nanomaterials after hydrothermal treatment [31,32]. The EDS analysis showed that the as-synthesized TNTs contained 72.5% Ti, 25.7% O and a small amount of Na (1.8%), suggesting that the chemical structure of as-synthesized TNTs was $Na_xH_{2-x}Ti_3O_7{\cdot}nH_2O$. After calcination at 500 °C and photo-deposition of Cu ions, a new peak at 25.3° 2θ, which can be assigned as the (1 0 1) orientation of anatase TiO_2 (JCPDS 21-1272), was found. In addition, several new small peaks centered at 24.6°, 29.7°, 32.9°, and 44.3° 2θ appeared in XRD patters of Cu-deposited TiO_2/TNTs, presumably attributed to the formation of TiO_2(B) [33]. However, no peak of Cu-based nanoparticles was observed because of the low added amount of Cu(II) ions (0.5–2 wt%). The XPS was further used to confirm the species of Cu ions in Cu-deposited TiO_2/TNTs. After deconvolution of Cu $2p_{3/2}$ XPS spectra shown in Fig. 2b, peaks centered at 933.6 and 932.7 eV, which can be assigned as CuO and Cu_2O, respectively, were clearly obtained, indicating the formation of mixture of Cu_2O and CuO (Cu_xO). It is noteworthy that both CuO and Cu_2O can absorb visible light. Therefore, the diffuse reflectance UV–vis spectrometry was used to characterize the optical property of Cu-deposited TiO_2/TNTs. Fig. S2 shows the UV–vis spectra of Cu-deposited TiO_2/TNT nanocomposites. The absorbance of Cu-deposited TiO_2/TNTs started to increase at 600–620 nm and the intensity increase upon increasing Cu amounts from 0.5 to 2 wt%, indicating that Cu(II) ions were photo-deposited onto the surface of TiO_2/TNTs to form Cu_xO for UV and visible light absorbance.

Fig. 3 shows the nitrogen adsorption–desorption isotherms and pore size distribution of the as-synthesized TNTs and Cu-deposited TiO_2/TNTs. The adsorption isotherm of as-synthesized TNTs showed a typical type IV isotherm with H3 hysteresis loop in the relative pressure (P/P_0) range of 0.5–0.8, indicating the characteristics of mesoporous materials. The calcination of as-synthesized TNTs increased the pore diameter, and resulted in

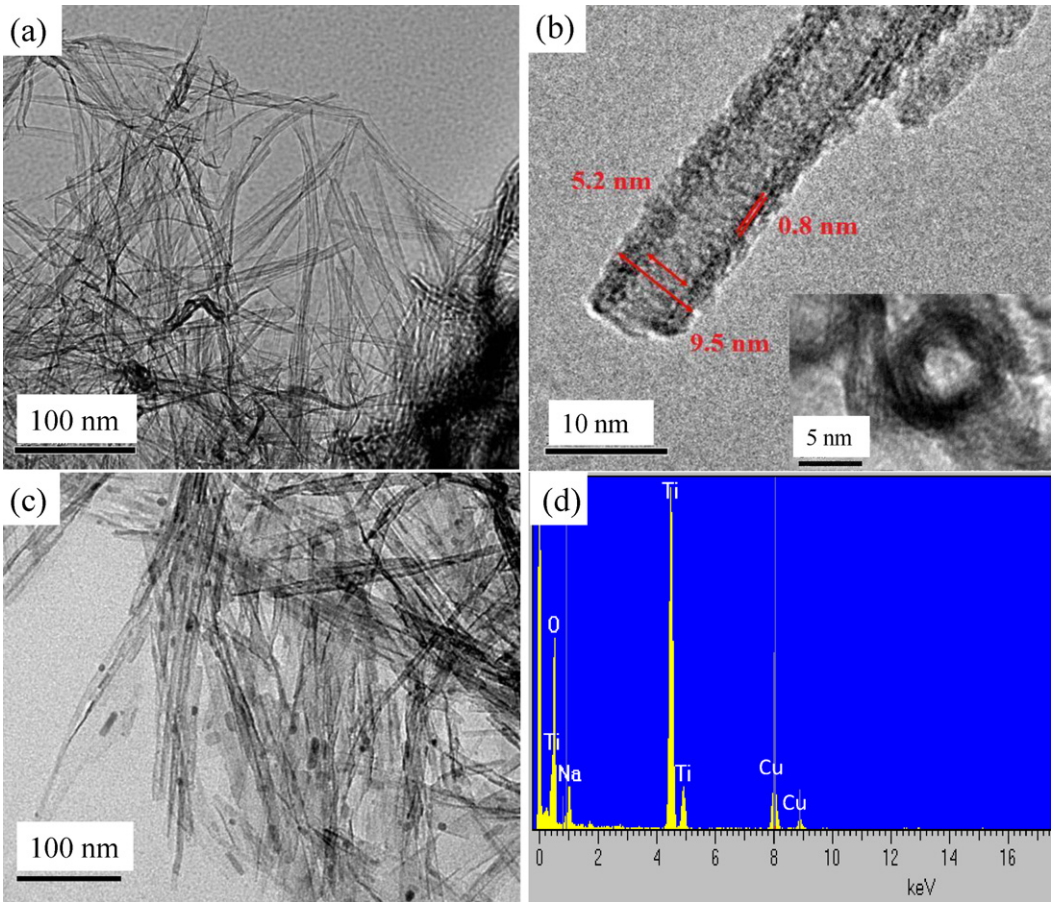

Fig. 1. TEM images of the as-synthesized TNTs and 1 wt% Cu-deposited TiO_2/TNTs. (a) and (b) are TEM and HRTEM images of as-synthesized TNTs, while (c) and (d) are the TEM images and EDS analysis of 1 wt% Cu-deposited TiO_2/TNTs, respectively.

the shift in hysteresis loops to the high relative pressure region of 0.8–0.95. The pore size distribution of as-synthesized and Cu-deposited TiO_2/TNTs, derived from the BJH method, showed that the average pore diameters were 4.6 and 5.2 nm, respectively. It is noteworthy that the surface area and pore size of ST01 TiO_2 were 305 m^2/g and 12.7 nm, respectively. When TiO_2 nanoparticles were transformed to the tubular structures during the hydrothermal processes, the specific surface area increased to 420 m^2/g. After calcination at 500 °C and deposition of Cu ions, however, the specific surface area decreased dramatically to 98 m^2/g because of the collapse of tubular structures and production of crystalline phase of anatase TiO_2 and mixture of CuO and Cu_2O, which is in good agreement with the TEM images.

XANES was used to understand the local symmetry of titanium and copper ions of the hydrothermal products. Fig. 4 shows the Ti K-edge and Cu $L_{2,3}$-edge XANES spectra for the as-synthesized TNTs and Cu-deposited TiO_2/TNTs. For Ti K-edge spectra, the characteristic peaks in the pre-edge region of 4965–4976 eV, denoted as P_1, P_2, P_3, and P_4, corresponded to the transitions from core 1s level to unoccupied 3d states (Fig. 4a) [34–36]. The origin of peak P_1 was assigned as an exciton band or a transition from $1s \rightarrow t_{1g}$, and is believed to be associated with Ti 3d–4p hybridized states. Peaks P_2 and P_4 were attributed to the $1s \rightarrow 3d$ transition and were designated as $1s \rightarrow t_{2g}$ and $1s \rightarrow 3e_g$ transitions, respectively [35,36]. The pre-edge spectrum of as-synthesized TNTs contained three major features, peaks P_1, P_2 and P_4, with the strong peak located at 4970.7 eV (peak P_2), which was the transition of $1s \rightarrow t_{2g}$ for tetrahedral symmetry [35]. On the contrary, the pre-edge spectrum of Cu-deposited TiO_2/TNTs contained peaks P_1, P_3, and P_4 with a notable blue shift from peak P_2 to peak P_3, reflecting the distortion of the octahedral TiO_6 unit. In addition, the peak P_4 was a pure dipolar component and provided a sensitive probe for the degree of distortion [34]. The increase in peak P_4 intensity in Cu-deposited TiO_2/TNTs also indicated the distortion around the TiO_6 octahedral sites.

In the main-edge region of 4976–4995 eV, three spectral features (denoted as A, B and C) corresponding to the dipole-allowed $1s \rightarrow 4p$ transitions were clearly observed [34,36]. The main-edge of as-synthesized TNTs showed small signals of peaks B and C, which was in good agreement with that of layered titanate nanohybrids doped with metal oxides [36,37]. In contrast, the main-edge spectral feature for the Cu-deposited TiO_2/TNTs changed and peak B at 4986.5 eV became obvious after the thermal treatment at 500 °C, which was similar to that of anatase TiO_2. This observation provides a strong support on the local structural change from layered trititanate to anatase TiO_2 through the distortion of TiO_6 units after calcination at 500 °C and photodeposition of Cu ions [32].

The Cu $L_{2,3}$-edge absorption spectra for Cu-deposited TiO_2/TNTs before and after UV light illumination are displayed in Fig. 4b. The strong peaks in the L_2 and L_3 areas centered at about 931 and 952 eV were mainly attributed to the inherent divalent copper states, which can be interpreted as the transition of $Cu(2p_{3/2})3d^9$ ground state to $Cu(2p_{3/2})^{-1}3d^{10}$ excited state [38]. After illumination with UV light to photo-deposit Cu ions, an additional small peak shown at about 934 eV was the Cu(I) L_3-edge resulting from the transition of $Cu(2p_{3/2})3d^{10}$ ground state to $Cu(2p_{3/2})^{-1}3d^{10}4s$,

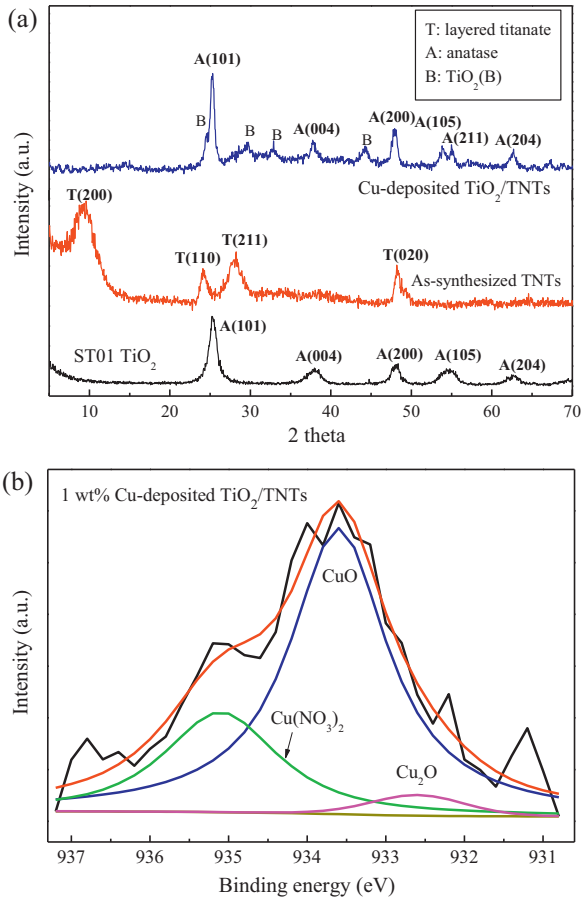

Fig. 2. (a) XRD patterns and (b) XPS spectra of the as-synthesized TNTs and 1 wt% Cu-deposited TiO_2/TNTs.

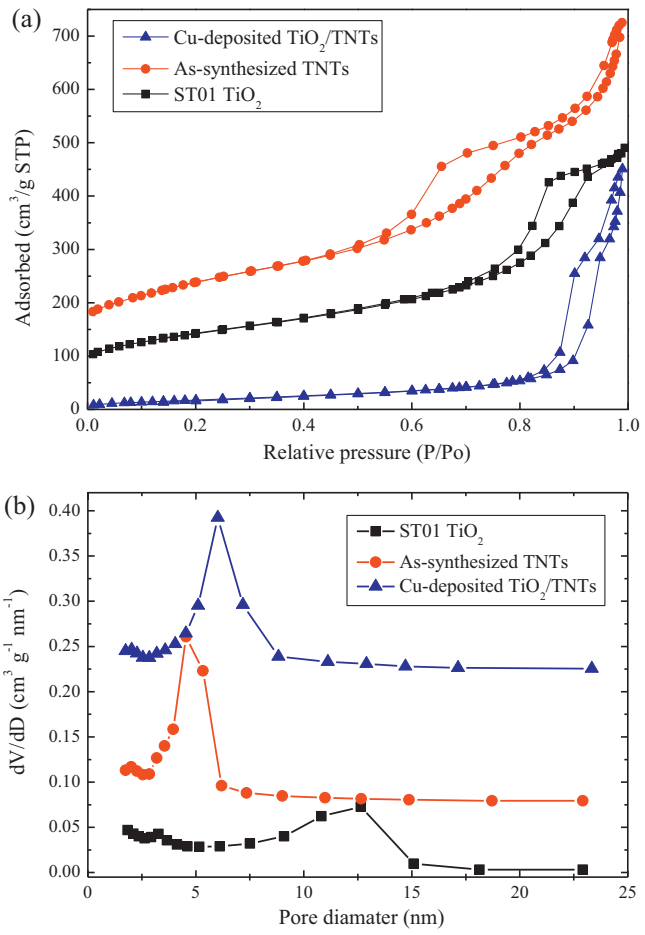

Fig. 3. (a) Nitrogen adsorption–desorption isotherms and (b) pore size distribution of ST01 TiO_2, as-synthesized TNTs and 1 wt% Cu-deposited TiO_2/TNTs. The adsorption isotherms for ST01 TiO_2 and as-synthesized TNTs are vertically shifted 60 and 130 cm^3 STP g^{-1}, respectively, for clarity.

which was originally from the level of oxygen-depleted Cu_xO after photo-induced conversion.

3.2. Photocatalytic activity of Cu-deposited TiO_2/TNTs

The photocatalytic activity of as-synthesized and Cu-deposited TiO_2/TNTs was evaluated using BPA as the target compound. Fig. 5 shows the photocatalytic degradation of BPA by various titanium-based nanomaterials under the illumination of 365 nm UV light at pH 7.0. No obvious photodegradation of BPA was observed after illumination of UV light for 90 min in the absence of TNTs (direct photolysis). Similar to the direct photolysis, less than 10% of BPA was photodegraded by as-synthesized TNTs. After post-thermal treatment at 500 °C, 40% of the original BPA was photodegraded within 90 min, depicting the increase in photocatalytic activity of TNTs after calcination. The commercial TiO_2 nanoparticles also showed good photocatalytic activity towards BPA degradation, and the removal efficiencies of 92% and 70% were observed within 90 min when Degussa P25 and ST01 TiO_2, respectively, were added.

The deposition of Cu(II) significantly enhanced the photocatalytic activity of TiO_2/TNT towards BPA degradation, and the photodegradation efficiency of BPA increased to >99.9% when 0.5–2 wt% Cu(II) was deposited. The k_{obs} for BPA photodegradation increased from 0.0074 min^{-1} in the absence of Cu(II) to 0.083 ± 0.004 min^{-1} at 0.5 wt% Cu(II) and then reached the maximum value of 0.253 ± 0.032 min^{-1} at 1 wt% Cu(II). After increasing the Cu(II) amount to 2 wt%, the k_{obs} values for BPA photodegradation slightly decreased to 0.137 ± 0.017 min^{-1}. It is noted that the k_{obs} for BPA photodegradation by P25 and ST01 TiO_2 were 0.049 and 0.02 min^{-1}, respectively. This means that the k_{obs} values for BPA photodegradation by Cu-deposited TiO_2/TNTs are 1.7–5.2 and 4.3–12.7 times higher than those of pure Degussa P25 and ST01 TiO_2, respectively, clearly showing the superior photoactivity of Cu-deposited TiO_2/TNTs towards photodegradation of BPA. In addition, 35% of TOC were removed after illumination of 120 min when 10 mg/L BPA was photodegraded by Cu-deposited TiO_2/TNT, which is higher than that by pure Degussa P25 TiO_2 (21%). These results clearly indicate that Cu-deposited TiO_2/TNTs is a promising nanomaterial which can effectively enhance the photo-mineralization efficiency of BPA under the illumination of 365 nm UV light.

The Cu(II) ions have different effects on commercial TiO_2 nanoparticles. As shown in Fig. S3, addition of 1 wt% Cu(II) slightly lowered the photodegradation efficiency and rate of BPA by Degussa P25 TiO_2 after 60 min of UV illumination. However, the photodegradation efficiency and rate of BPA by ST01 increased when 1 wt% Cu(II) was added. This discrepancy is mainly attributed to the different compositions of TiO_2 between P25 and ST01. The P25 TiO_2 contains 80% anatase and 20% rutile, which could form interparticle electron transfer (IPET) to enhance the photocatalytic activity of TiO_2. The addition of Cu(II) has little effect on IPET and may block the photoreactive sites of P25 TiO_2, resulting in the decrease in the photodegradation efficiency and rate of BPA. In contrast, ST01 contains 100% anatase TiO_2 and the formation of Cu_xO enhances the electron–hole separation efficiency. It is noteworthy that the k_{obs} for BPA photodegradation was 0.041 min^{-1} for P25-Cu_xO and 0.023 min^{-1} for ST01-Cu_xO, which were 6.3–11 times lowered than that of 1 wt% Cu-deposited TiO_2/TNTs, clearly

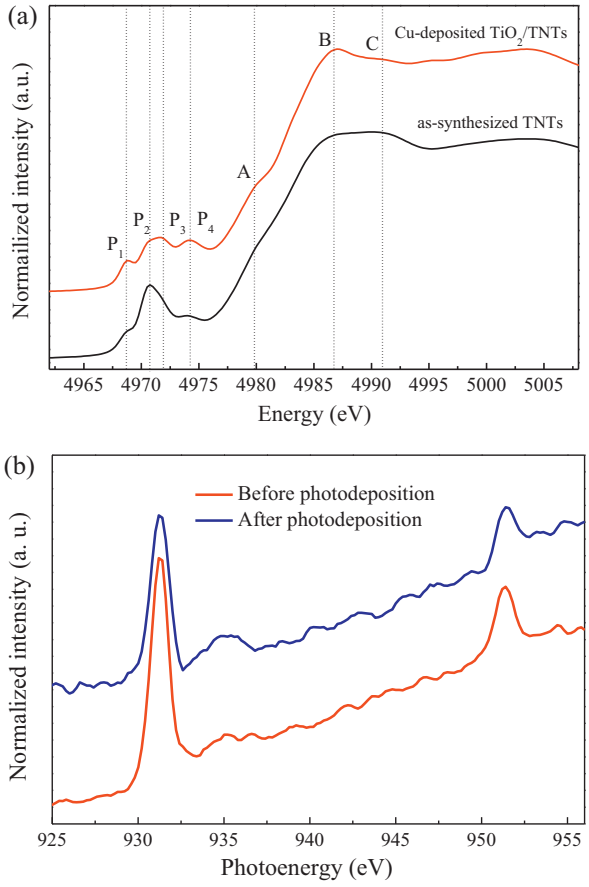

Fig. 4. The (a) Ti K-edge and (b) Cu $L_{2,3}$-edge XANES spectra of the as-synthesized TNTs and Cu-deposited TiO_2/TNTs.

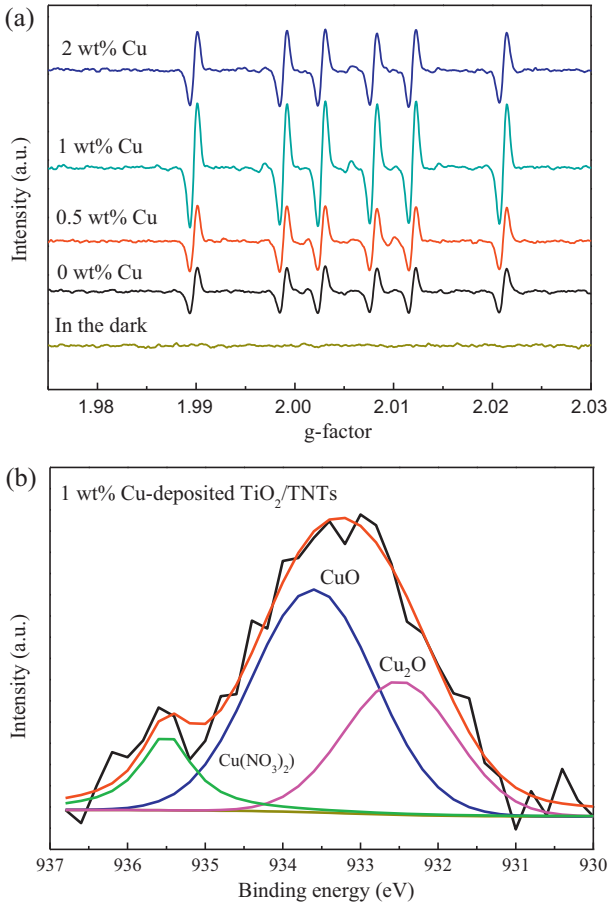

Fig. 6. The (a) EPR and (b) XPS spectra of the Cu-deposited TiO_2/TNTs obtained from the illumination of UV light for 5 min in the presence of 10 mg/L BPA.

showing that addition of Cu(II) ions has a significant effect on the enhanced photocatalytic activity of TiO_2/TNT nanocomposites towards BPA photodegradation compared with those of commercial TiO_2 nanoparticles.

3.3. Possible reaction mechanism for photodegradation

In this study, we have found that the photocatalytic activity of 1D TNTs towards BPA photodegradation can be significantly enhanced after photodeposition of copper ions. It is believed that the photodegradation of BPA may involve several steps initiated from the photo-generation of electrophilic hydroxyl radicals and/or O-centered radical adducts [27,29,39]. Fig. 6 shows the EPR spectra of free radicals and XPS spectrum of Cu species after the illumination of Cu-deposited TiO_2/TNTs. As illustrated in Fig. 6a, no EPR signal was produced in solutions containing DMPO and Cu-deposited TiO_2/TNTs in the presence of 10 mg/L BPA in the dark. After illumination of Cu-deposited TiO_2/TNTs with UV light for 5 min, the six-line EPR spectra were clearly observed, indicating the generation of O-centered radical adducts such as •OH, •OOH, and ROO• [40,41]. In addition, the EPR intensity increased upon increasing the Cu amount from 0.5 to 1 wt% and then slightly decrease at 2 wt% Cu, clearly showing that addition of copper ion is conducive to the production of radicals. The deconvolution of Cu $2p_{3/2}$ XPS spectrum clearly indicated the formation of CuO (933.6 eV) and Cu_2O (932.7 eV) after the illumination of Cu-deposited TiO_2/TNTs for 5 min (Fig. 6b). The ratio of Cu_2O to total Cu species (CuO + Cu_2O), determined by the peak areas of Cu_2O and total $Cu2p_{3/2}$ species, increased from 3.2% in the dark (Fig. 2b) to 35.2% after the illumination of UV light. This result clearly indicates that Cu species can be reduced to low-valent Cu species during photocatalytic reaction, and subsequently enhances the separation efficiency of holes and electrons. It is noteworthy that Cu_2O can easily be oxidized to form a layer of CuO once exposed to the ambience and the XPS data can only represent the surface information, which indicates that the real content of Cu_2O in the nanocomposites remains unclear. The use of HRTEM with selected area electron diffraction would be conductive to characterize the nanoparticles of Cu-deposited

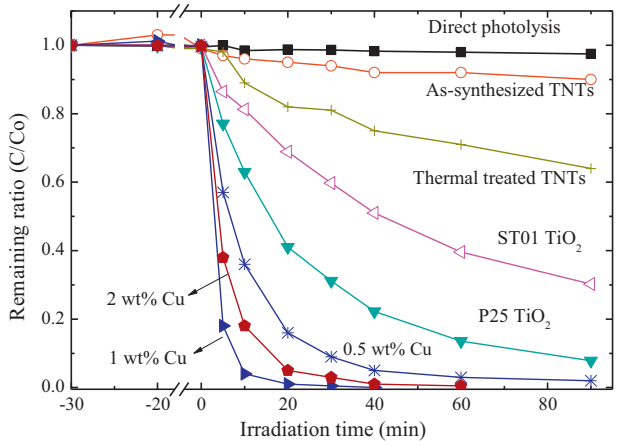

Fig. 5. The photodegradation of 10 mg/L BPA by various titanium-based nanomaterials under the illumination of 365 nm UV light at pH 7 and at 25 °C.

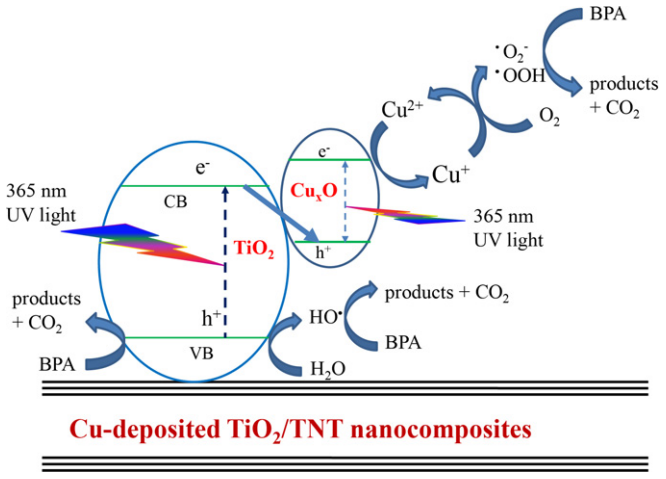

Scheme 1. The possible reaction mechanism for photocatalytic degradation of BPA by Cu-deposited TiO_2/TNTs under illumination of 35 nm UV light.

TiO_2/TNTs for better understanding the real content of copper (I,II) oxides in the nanocomposites.

Scheme 1 illustrates the possible reaction mechanisms for photocatalytic degradation of BPA by Cu-deposited TiO_2/TNTs. When both TiO_2/TNTs and Cu_xO absorbs UV light, which the energy is higher than its bandgap, electron/hole pairs are generated (Eqs. (3) and (4)). The generated electrons from TiO_2 with a lower conduction band could recombine with the hole in Cu_xO, resulting in the formation of Cu(I) species as well as in the reduction of recombination rate of electrons and holes of TiO_2/TNTs. The Cu(I) species was again converted to Cu(II) and superoxide anion radicals ($^{\bullet}O_2^-$) in the presence of oxygen (Eqs. (5) and (6)). In addition, the holes and electrons reacted with water and oxygen, respectively, to form peroxyl and hydroxyl radicals on the surface of Cu-deposited TiO_2/TNTs (Eqs. (7) and (9)), resulting in the enhancement of the photodegradation efficiency and rate of BPA by Cu-deposited TiO_2/TNTs (Eqs. (10) and (11)).

$$TiO_2/TNTs + h\upsilon \rightarrow e^- + h^+ \quad (3)$$

$$Cu_xO + h\upsilon \rightarrow e^- + h^+ \quad (4)$$

$$Cu_2 + e^-_{(TiO_2)} \rightarrow Cu^+ \quad (5)$$

$$Cu^+ + O_2 \rightarrow Cu^{2+} + {}^{\bullet}O_2^- \quad (6)$$

$$O_2 + e^- \rightarrow {}^{\bullet}O_2^- \quad (7)$$

$$^{\bullet}O_2^- + H^+ \rightarrow HO_2^{\bullet} \quad (8)$$

$$H_2O + h^+ \rightarrow {}^{\bullet}OH + H^+ \quad (9)$$

$$BPA + h^+ \rightarrow BPA^+ \rightarrow \text{products} + CO_2 \quad (10)$$

$$BPA + {}^{\bullet}OH(\text{or}{}^{\bullet}OOH) \rightarrow \text{products} + CO_2 \quad (11)$$

4. Conclusions

In this study, we have first demonstrated the enhanced effect of copper ions on the photocatalytic degradation of BPA by 1D TNTs under illumination of 365 nm UV light. The as-synthesized TNTs showed tubular structures and the well-crystallized anatase TiO_2 and Cu_xO nanoparticles were produced on the tube walls to form Cu-deposited TiO_2/TNT nanocomposites after calcination and photodeposition. The Cu-deposited TiO_2/TNTs exhibited an enhanced effect on the photocatalytic degradation of BPA, and the k_{obs} for BPA photodegradation by Cu-deposited TiO_2/TNTs increased by factors of 1.8–5.2 and 4.3–12.7 when compared with those of P25 and ST01 TiO_2, respectively. Electron spin resonance results showed that addition of copper ions could serve as the electron mediators to prolong to retention time of photo-generated radicals, resulting in the enhancement of photodegradation efficiency and rate of BPA by Cu-deposited TiO_2/TNTs. Results obtained in this study open an avenue to apply 1D nanostructured titanates for effective degradation of toxic chemicals in the aqueous solutions.

Acknowledgements

The authors thank the National Science Council, Taiwan for financial support under Contract Nos. NSC 98-2221-E-007-030-MY3 and NSC 99-2627-M-007-006.

Appendix A. Supplementary data

Supplementary data associated with this article can be found, in the online version, at http://dx.doi.org/10.1016/j.apcatb.2012.09.011.

References

[1] R.A. Doong, I.L. Kao, Recent Patents on Nanotechnology 2 (2008) 84–102.
[2] H.B. Wu, X.W. Lou, H.H. Hng, Chemistry: A European Journal 18 (2012) 2094–2099.
[3] Y.C. Chen, S.L. Lo, J. Kuo, Water Research 45 (2011) 4131–4140.
[4] D.V. Bavykin, J.M. Friedrich, F.C. Walsh, Advanced Materials 18 (2006) 2807–2824.
[5] J.G. Yu, Q.L. Li, J.J. Fan, B. Cheng, Chemical Communications 47 (2011) 9161–9163.
[6] H.U. Ou, S.L. Lo, Separation and Purification Technology 58 (2007) 179–191.
[7] C.C. Tsai, H. Teng, Langmuir 24 (2008) 3434–3438.
[8] R.A. Doong, L.F. Chiang, Water Science and Technology 58 (2008) 1985–1992.
[9] N. Murakami, Y. Fujisawa, T. Tsubota, T. Ohno, Applied Catalysis B: Environmental 92 (2009) 56–60.
[10] L. Xiong, W.L. Sun, Y. Yang, C. Chen, J.R. Ni, Journal of Colloid and Interface Science 356 (2011) 211–216.
[11] X.P. Wang, Y.X. Tang, M.Y. Leiw, T.T. Lim, Applied Catalysis A: General 409 (2011) 257–266.
[12] Q. Wu, J.J. Quyang, K.P. Xiea, L. Sun, M.Y. Wang, C.J. Lin, Journal of Hazardous Materials 199 (2012) 410–417.
[13] R.A. Doong, P.Y. Chang, C.H. Huang, Journal of Non-Crystalline Solids 355 (2009) 2302–2308.
[14] G.K. Parshetti, R.A. Doong, Applied Catalysis B: Environmental 100 (2010) 116–123.
[15] M. Hamadanian, A. Reisi-Vanani, A. Majedi, Applied Surface Science 256 (2010) 1837–1844.
[16] R.A. Doong, T.C. Hsieh, C.P. Huang, Science of the Total Environment 408 (2010) 3334–3341.
[17] H.Q. An, J.A. Zhou, J.X. Li, B.L. Zhu, S.R. Wang, S.M. Zhang, S.H. Wu, W.P. Huang, Catalysis Communications 11 (2009) 75–79.
[18] J.G. Yu, Q.J. Xiang, M.H. Zhou, Applied Catalysis B: Environmental 90 (2009) 595–602.
[19] S. Chatterjee, K. Bhattacharyya, P. Ayyub, A.K. Tyagi, The Journal of Physical Chemistry C 114 (2010) 9424–9430.
[20] S.K. Khanal, B. Xie, M.L. Thompson, S.W. Sung, S.K. Ong, J. Van Leeuwen, Environmental Science and Technology 40 (2006) 6537–6546.
[21] C. Ort, M.G. Lawrence, J. Rieckemann, A. Joss, Environmental Science and Technology 44 (2010) 6024–6035.
[22] L.B. Barber, A.M. Vajda, C. Douville, D.O. Norris, J.H. Writer, Environmental Science and Technology 46 (2012) 2121–2131.
[23] I.B. Toledo, M.A. Ferro-Garcia, J. Rivera-Utrilla, C. Moreno-Castilla, F.J.V. Fernandez, Environmental Science and Technology 39 (2005) 6246–6250.
[24] P. Westerhoff, Y. Yoon, S. Snyder, E. Wert, Environmental Science and Technology 39 (2005) 6649–6663.
[25] I. Oller, S. Malato, J.A. Sanchez-Perez, The Science of the Total Environment 409 (2011) 4141–4166.
[26] M. Klavarioti, D. Mantzavinos, D. Kassinos, Environment International 35 (2009) 402–417.
[27] N. Watanabe, S. Horikoshi, H. Kawabe, Y. Sugie, J.C. Zhao, H. Hidaka, Chemosphere 52 (2003) 851–859.
[28] C.Y. Wang, H. Zhang, F. Li, L.Y. Zhu, Environmental Science and Technology 44 (2010) 6843–6848.
[29] C.S. Guo, M. Ge, L. Liu, G.D. Gao, Y.C. Feng, Y.Q. Wang, Environmental Science and Technology 44 (2010) 419–425.
[30] D.P. Subagio, M. Srinivasan, M. Lim, T.T. Lim, Applied Catalysis B: Environmental 95 (2010) 414–422.
[31] S. Zhang, Q. Chen, L.M. Peng, Physical Review B 71 (2005) 014104.
[32] D.L. Morgan, H.W. Liu, R.L. Frost, E.R. Waclawik, The Journal of Physical Chemistry C 114 (2010) 101–110.

[33] M. Qamar, C.R. Yoon, H.J. Oh, D.H. Kim, J.H. Jho, K.S. Lee, W.J. Lee, H.G. Lee, S.J. Kim, Nanotechnology 17 (2006) 5922–5929.
[34] G. Fronzoni, R. De Francesco, M. Stener, M. Causa, The Journal of Physical Chemistry B 110 (2006) 9899–9907.
[35] A. Nakahira, T. Kubo, C. Numako, Inorganic Chemistry 49 (2010) 5845–5852.
[36] T.W. Kim, H.W. Ha, M.J. Paek, S.H. Hyun, I.H. Baek, J.H. Choy, S.J. Hwang, The Journal of Physical Chemistry C 112 (2008) 14853–14862.
[37] T.W. Kim, H.W. Ha, M.J. Paek, S.H. Hyun, J.H. Choy, S.J. Hwang, Journal of Materials Chemistry 20 (2010) 3238–3245.
[38] Y. Tanaka, M. Karppinen, T. Kobayashi, T.S. Chan, R.S. Liu, J.M. Chen, H. Yamauchi, Chemistry of Materials 20 (2008) 5414–5420.
[39] C.Y. Kuo, C.H. Wu, H.Y. Lin, Desalination 256 (2010) 37–42.
[40] C.M. Jones, M.J. Burkitt, Journal of the American Chemical Society 125 (2003) 6946–6954.
[41] H.J. Zhang, G.H. Chen, Environmental Science and Technology 43 (2009) 2905–2910.